



1 **Interpretation of NO₃-N₂O₅ observation via steady state in high aerosol air**
2 **mass: The impact of equilibrium coefficient in ambient conditions**

3 Xiaorui Chen¹, Haichao Wang^{3,4}, Keding Lu^{1,2}

4 ¹State Key Joint Laboratory of Environmental Simulation and Pollution Control, College of
5 Environmental Sciences and Engineering, Peking University, Beijing, China.

6 ²The State Environmental Protection Key Laboratory of Atmospheric Ozone Pollution Control

7 ³School of Atmospheric Sciences, Sun Yat-sen University, Zhuhai, 519082, China

8 ⁴Guangdong Provincial Observation and Research Station for Climate Environment and Air
9 Quality Change in the Pearl River Estuary, Key Laboratory of Tropical Atmosphere-Ocean
10 System, Ministry of Education, Southern Marine Science and Engineering Guangdong
11 Laboratory (Zhuhai), Zhuhai, 519082, China

12 *Correspondence to:* Haichao Wang (wanghch27@mail.sysu.edu.cn), Keding Lu
13 (k.lu@pku.edu.cn)

14

15 **Abstract.** Steady state approximation for interpreting NO₃ and N₂O₅ has large uncertainty
16 under complicated ambient conditions and could even produces incorrect results
17 unconsciously. To provide an assessment and solution to the dilemma, we formulate data sets
18 based on in-situ observations to reassess the applicability of the method. In most of steady
19 state cases, we find a prominent discrepancy between *Keq* (equilibrium coefficient for
20 reversible reactions of NO₃ and N₂O₅) and correspondingly simulated $[N_2O_5]/([NO_2] \times [NO_3])$,
21 especially in wintertime high aerosol conditions. This gap reveals the accuracy of *Keq* has a
22 critical impact on the steady state analysis in polluted region. In addition, the accuracy of
23 $\gamma(N_2O_5)$ derived by steady state fit depends closely on the reactivity of NO₃ (*k*NO₃) and N₂O₅
24 (*k*N₂O₅). Based on a complete set of simulations, air mass of *k*NO₃ less than 0.01 s⁻¹ with high
25 aerosol and temperature higher than 10°C is suggested to be the best suited for steady state
26 analysis of NO₃-N₂O₅ chemistry. Instead of confirming the validity of steady state by
27 numerical modeling for every case, this work directly provides concentration ranges
28 appropriate for accurate steady state approximation, with implications for choosing suited
29 methods to interpret nighttime chemistry in high aerosol air mass.

30



31 **1 Introduction**

32 Nitrate radical (NO_3), an extremely reactive species prone to build up at night, is an ideal
33 candidate for steady state analysis in combine with dinitrogen pentoxide (N_2O_5) due to fast
34 equilibrium reactions between them (R1).



35 Numerous works have taken the advantage of the steady state calculation to quantify the total
36 first-order loss rate for NO_3 or N_2O_5 such that they drew conclusions about the oxidation
37 capacity and reactive nitrogen budgets contributed by this chemical system (Allan et al.,
38 1999; Allan et al., 2000; Carslaw et al., 1997; Platt et al., 1984; Vrekoussis et al., 2007; Wang et
39 al., 2013). Since the steady state approximation was extended to interpret atmospheric
40 observation of NO_3 - N_2O_5 by Brown et al. (2003), this method has been widely implemented
41 to quantify N_2O_5 uptake coefficient ($\gamma(\text{N}_2\text{O}_5)$) (Brown et al., 2009; Brown et al., 2003; Li et al.,
42 2020; McDuffie et al., 2019; Phillips et al., 2016; Wang et al., 2017a; Wang et al., 2017c).

43 However, with the influence induced by complicated atmospheric conditions and
44 emission, the steady state in ambient air mass will not always be the case (as illustrated in Text
45 S1 and Figure S1). These situations are prevalent in nocturnal boundary layer (Phillips et al.,
46 2016; Stutz et al., 2004; Wang et al., 2017a; Wang et al., 2017c) and therefore increase the
47 difficulty of applying steady state directly on NO_3 - N_2O_5 observation data, whereas few studies
48 have systematically characterized the error source and application conditions of this method
49 (Brown et al., 2009).

50 Due to faster approach to equilibrium than steady state, the application of equilibrium
51 coefficient (K_{eq}) in calculation steady state equations seems to be reasonable (Brown et al.,
52 2003). For example, the ambient NO_3 concentration was usually calculated based on ambient
53 N_2O_5 concentration with $K_{\text{eq}} \times [\text{NO}_2]$ when determining their budgets or characterizing the
54 lifetime or sink attribution of these two reactive nitrogen compounds (Brown et al.,
55 2011; Osthoff et al., 2006; Wang et al., 2018b; Wang et al., 2017c; Wang et al., 2017d). In
56 addition, the concentration conversion between NO_3 and N_2O_5 via K_{eq} coefficient can
57 simplified the calculation in the iterative box model, which is proposed to quantify $\gamma(\text{N}_2\text{O}_5)$
58 (Wagner et al., 2013). However, considerable uncertainty could be associated with the
59 quantification of K_{eq} and its different parameterizations (Cantrell et al., 1988; Pritchard, 1994).
60 The impact of K_{eq} value on steady state fit or concentration conversion have not been explored
61 to date in the analysis of NO_3 - N_2O_5 steady state.

62 In this study, we formulate a half artificial dataset with expected properties based on field



63 campaigns. With the dataset, we illustrate the reasons for K_{eq} values distinct from
64 parameterization in ambient conditions, the possible uncertainties of linear fit resulted from
65 different K_{eq} , and the influence of other atmospheric variables on $\gamma(N_2O_5)$ derivation via
66 steady state method. Furthermore, a series of ambient condition tests specify the exact ranges
67 suited for steady state analysis according to not only the validity of steady state but also K_{eq}
68 values, which optimizes the validity check by numerical modeling in previous research
69 (Brown et al., 2009; Brown et al., 2003) and develops complete standard for data filtering.

70 **2 Methods**

71 **2.1 $\gamma(N_2O_5)$ derivation by steady state approximation**

72 The framework of steady state calculation for NO_3 - N_2O_5 system is basically built on its
73 chemical production and removal pathways, in the case of extremely weak physical processes
74 relative to its chemical processes. With simultaneous measurements of NO_3 , N_2O_5 and relevant
75 precursor concentrations, the steady state lifetime $\tau_{ss}(NO_3)$ and $\tau_{ss}(N_2O_5)$ can be
76 quantified for a given analysis period, and yield $\gamma(N_2O_5)$ and the reactivity of NO_3 (k_{NO_3} ,
77 including the reactions of NO_3 with NO and hydrocarbons) based on Eq. (1) and Eq. (2).

$$78 \quad \tau_{ss}^{-1}(NO_3) \approx k_{NO_3} + 0.25cS_aK_{eq}[NO_2]\gamma(N_2O_5), \quad (1)$$

$$79 \quad (0.25cS_a\tau_{ss}(N_2O_5))^{-1} \approx \gamma(N_2O_5) + k_{NO_3}(0.25cS_aK_{eq}[NO_2])^{-1}, \quad (2)$$

80 Here c represents the mean molecular velocity of N_2O_5 , S_a represents the aerosol surface area
81 and the K_{eq} is calculated from the rate constant of reversible reactions R1a (k_{R1a}) and R1b
82 (k_{R1b}), which is a temperature-dependent parameter. In the form of these two equations, the
83 potential covariance between S_a and NO_2 concentration can be avoided to decrease the
84 uncertainty (Brown et al., 2009). By fit to these two equations, $\gamma(N_2O_5)$ can be directly derived
85 from slope of the plot of $\tau_{ss}^{-1}(NO_3)$ against $0.25cS_aK_{eq}[NO_2]$ or from intercept of the plot
86 of $(0.25cS_a\tau_{ss}(N_2O_5))^{-1}$ against $(0.25cS_aK_{eq}[NO_2])^{-1}$ respectively. In the following
87 analysis, the linear fitting based on Eq. (2) is preferred in steady state approximation.



88 2.2 Steady state model and half-artificial datasets

89 A half-artificial dataset can be provided by a steady state framework model, extended from 0-
90 dimension box model, where steady state of NO_3 and N_2O_5 is valid for each data point. As
91 NO_3 - N_2O_5 chemistry, the interest of this work, usually shows marked impacts during the night,
92 the data set includes only the time periods when photolysis rates are negligible. The model
93 runs are constrained by measurements of NO , NO_2 , O_3 , CO , CH_4 , VOCs, HCHO, Sa, relative
94 humidity (RH), temperature (T), pressure, coupled with Regional Atmospheric Chemistry
95 Mechanism, version 2 (RACM2). Other details on the species surrogates and deposition rates
96 can be referred to previous study (Chen et al., 2019; Wang et al., 2018a).

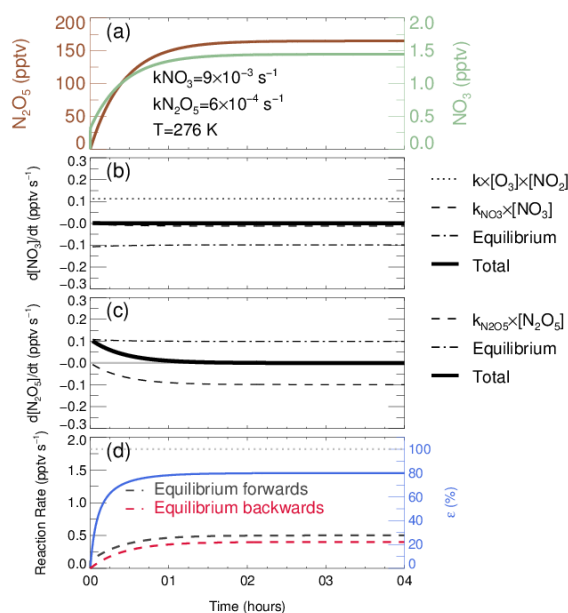
97 In the standard simulation (herein referred as Mod0), the uptake coefficient of N_2O_5 is set
98 to 0.02, as a reasonable value of literatures (Brown et al., 2006; Chen et al., 2020; McDuffie et
99 al., 2018; Morgan et al., 2015; Phillips et al., 2016; Wagner et al., 2013; Wang et al., 2017c; Yu
100 et al., 2020). Each data point is treated as an independent air mass, aging 10 hours without
101 illumination and keeping input constraint unchanged. The simulation results of these two half-
102 artificial datasets based on PKU2017 and TZ2018 field campaigns (see Text S2) show a large
103 variability of nocturnal air masses (see Text. S3 and Figure S2). We presume that if any data
104 point outputted from this model is still invalid for steady state, the sink rate constant of air
105 mass represented by this data point should be too weak for steady state analysis in ambient
106 conditions within a reasonable timescale. Data filtering according to Eq. (1) and Eq. (2)
107 restricts available data points not to deviate from steady state more than 10%. In addition, the
108 data higher than 5 ppbv NO is filtered out in the following calculation, since the resulting large
109 variation of $k\text{NO}_3$ can break the fitting even under the steady state (discussed in 3.2). Rather
110 than using observation data directly, replacing with half-artificial dataset can provide larger
111 amount of valid data for steady state analysis with known $\gamma(\text{N}_2\text{O}_5)$ value and avoid the impacts
112 from steady state deviation, which helps to analyze the factors influencing $\gamma(\text{N}_2\text{O}_5)$
113 quantification via steady state approximation backwards from a known steady state condition.



114 3 Results and discussion

115 3.1 Varying equilibrium coefficient under steady state

116 The rates of $\text{NO}_3\text{-N}_2\text{O}_5$ reversible reactions are expected to be equal for the steady state case,
 117 so that the equilibrium coefficient K_{eq} can be determined from either the rate constant ratio of
 118 R1a and R1b or the ratio of $[\text{N}_2\text{O}_5]/([\text{NO}_2] \times [\text{NO}_3])$. Although this approach is reasonable
 119 under ideal conditions, the exactly same rates between reversible reactions and the following
 120 calculation based on K_{eq} scaling are not so appropriate for ambient atmosphere where the
 121 removal pathway for $\text{NO}_3\text{-N}_2\text{O}_5$ are not negligible, especially under the high aerosol loading
 122 condition. The $\text{NO}_3\text{-N}_2\text{O}_5$ achieves steady state after 1.5-hours evolution, when concentration
 123 and rates remain constant (Figure 1). Under steady state, the net equilibrium reaction rate in
 124 Figure 1(b)&(c) stays negative and positive for NO_3 and N_2O_5 respectively. Besides, the
 125 absolute values and difference of the forward and backward reaction rates remain unchanged
 126 after achieving steady state. This result is similar with a previous numerical calculation study
 127 (Brown et al., 2003), while the deviation between reversible reaction rates becomes larger in
 128 our case.



129 **Figure 1.** Evolution of $\text{NO}_3\text{-N}_2\text{O}_5$ system simulated by steady state model for an average case. (a) Temporal
 130 profiles of N_2O_5 and NO_3 , the constraint of simulation is displayed as the text; (b) Evolution of $d[\text{NO}_3]/dt$
 131 calculated from source of $k_{\text{O}_3+\text{NO}_2} \times [\text{O}_3] \times [\text{NO}_2]$, sink of $k_{\text{NO}_3} \times [\text{NO}_3]$ and equilibrium terms, detailed in
 132 the text; (c) Evolution of $d[\text{N}_2\text{O}_5]/dt$ calculated from equilibrium terms, sink of $k_{\text{N}_2\text{O}_5} \times [\text{N}_2\text{O}_5]$; (d) Forward
 133 (N_2O_5 formation) and backward (N_2O_5 decomposition) equilibrium rate are represented as black and red
 134

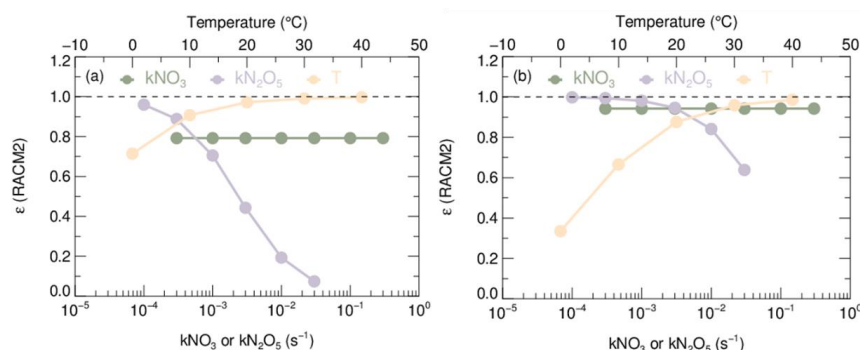


135 dash lines, the equilibrium completeness ε is calculated by the ratio of backward rate over forward rate,
136 shown as blue full line.

137 In this case, the original equilibrium is imperfect reached (the original equilibrium
138 condition is perfect reached as K_{eq} and the ratio of $[N_2O_5]/([NO_2] \times [NO_3])$ are equivalent),
139 leading to errors on projection of NO_3 and N_2O_5 concentration via $K_{eq} \times [NO_2]$. In fact, we
140 note that a new equilibrium between NO_3 and N_2O_5 is developed with constant but unequal
141 rates. Under this new equilibrium condition, the ratio of R1b reaction rate (the red dash line in
142 Figure1(d)) over R1a reaction rate (the black dash line in Figure1(d)) can be regarded as the
143 degree of approaching original equilibrium (the blue line in Figure1(d)). In addition, this value
144 is also the ratio of $[N_2O_5]/([NO_2] \times [NO_3])$ against original K_{eq} , therefore we defined this ratio
145 as a correction factor ε , implemented to calculate accurate $[N_2O_5]/([NO_2] \times [NO_3])$ with
146 significant NO_3 - N_2O_5 removal pathways. The value of K_{eq} after scaled by ε can be used for
147 converting the concentration of NO_3 and N_2O_5 via Eq. (3):

$$148 \quad \varepsilon \times K_{eq} = \varepsilon \times \frac{k_{R1a}}{k_{R1b}} = \frac{[N_2O_5]}{[NO_2][NO_3]}, \quad (3)$$

149 Sensitivity tests are conducted to demonstrate the dependence of ε on relevant variables
150 based on steady state model. The average ambient conditions observed at wintertime PKU site
151 and summertime TZ site are taken as basic constraint for sensitivity tests (Table S2),
152 respectively. By separately altering variables, such as NO_2 , O_3 , kN_2O_5 , kNO_3 and T, the
153 sensitivity of ε value can be obtained as shown in Figure 2 and Figure S4. The ε value
154 depends primarily on kN_2O_5 and T in both scenarios, where ε increases with T (approaching
155 1 under relatively high T) and decreases with kN_2O_5 . In comparison, the ε value behaves
156 insensitive to kNO_3 as well as NO_2 and O_3 concentration, at least within the range of reasonable
157 ambient conditions. High kN_2O_5 is resulted from high aerosol events, usually occur in winter
158 accompanied with low temperature and high relative humidity in some populated areas
159 (Baasandorj et al., 2017;Huang et al., 2014;Wang et al., 2017b;Wang et al., 2014), further
160 decreasing the accuracy of original K_{eq} values. It can be inferred that in order to accurately
161 interpreting relationship of NO_3 and N_2O_5 , calculation relying on equilibrium equation and
162 steady state approximation should consider the dependence of ε on ambient conditions.



163

164 **Figure 2.** Sensitivity plot of $k\text{NO}_3$, $k\text{N}_2\text{O}_5$ and Temperature (T) against coefficient ϵ . (a) Basic model
165 constraint is according to typical winter condition of PKU2017; (b) Basic model constraint is according to
166 typical summer condition of TZ2018. It should be noted that the provided ranges of each factor do not
167 exactly equal to but encompass the ambient conditions encountered during the two campaigns.

168 Even if K_{eq} value serves as a good representation of the ratio of $[\text{N}_2\text{O}_5]/([\text{NO}_2]\times[\text{NO}_3])$
169 or ϵ can be readily quantified on field, the discrepancy among different database in
170 calculating K_{eq} still increase the uncertainties of NO_3 - N_2O_5 calculation through steady state
171 approximation or equilibrium, which has not been carefully considered to date. Here, we apply
172 a set of uniform formulas to describing k_{R1a} and k_{R1b} (see Text. S4) from preferred values of
173 several popular atmospheric chemistry mechanisms (Mozart, CB05, Saprc07, RACM2 and
174 kinetic databases JPL2015 as well as IUPAC2017) and finally calculating K_{eq} . As is shown in
175 Figure S5, K_{eq} variations derived from these six different databases reflect considerable
176 discrepancy from each other, though they vary with consistent tendency. Because original K_{eq}
177 values are only dependent on ambient temperature, they continuously increase with time due
178 to the decrease of temperature. In addition to discrepancy between different K_{eq}
179 parameterizations, ϵ value varies dissimilarly with each K_{eq} , ranging from 70% to 90%. All
180 these results demonstrate that, in most cases, K_{eq} values simply derived from existing database
181 would fail to reproduce accurate relationship between NO_3 and N_2O_5 .

182 To further elucidate the impact of K_{eq} on deriving $\gamma(\text{N}_2\text{O}_5)$ via steady state approximation
183 (hereafter defined as $\gamma_{\text{ss}}(\text{N}_2\text{O}_5)$), Figure S6 shows the steady state fit based on all six database-
184 derived K_{eq} and in the same time periods as Figure S5 through Eq. (1) and Eq. (2) respectively
185 (both of equations can derive a pair of $\gamma_{\text{ss}}(\text{N}_2\text{O}_5)$ and $k\text{NO}_3$). The K_{eq} (corrected with ϵ) is
186 calculated with NO_3 and N_2O_5 concentration simulated based on RACM2. Fit based on Eq. (1)
187 could lead to 11~46% underestimation of $\gamma_{\text{ss}}(\text{N}_2\text{O}_5)$, as indicated by varying slopes in Figure
188 S6(b)&(d), when using the database-derived K_{eq} . Conversely, fit by Eq. (2) (shown in Figure
189 S6(a)&(c)) bias the result of $k\text{NO}_3$ served as the slopes without much influence on $\gamma_{\text{ss}}(\text{N}_2\text{O}_5)$

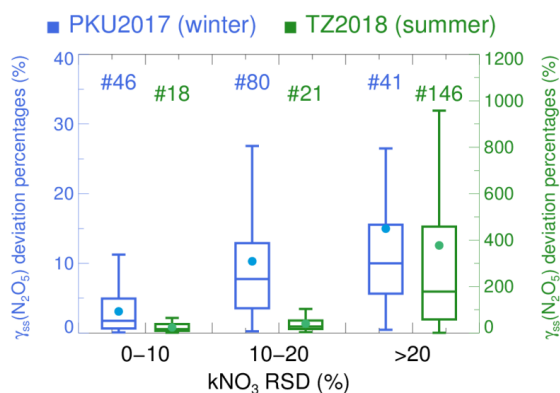


190 served as the intercept. Previous research ascribed inconsistent fit results between two
191 equations to measurements uncertainty (Brown et al., 2009; Brown et al., 2006). However, fit
192 with original K_{eq} might be the primary reasons for such inconsistent results, and even deviates
193 the derived $\gamma_{ss}(\text{N}_2\text{O}_5)$ and $k\text{NO}_3$ from true values. Therefore, steady state fit based on Eq. (2)
194 might be the best choice for $\gamma(\text{N}_2\text{O}_5)$ derivation via steady state approximation. Similarly, Eq.
195 (1) is preferred to be applied when $k\text{NO}_3$ is the final objective.

196 3.2 Impacts of $\text{NO}_3\text{-N}_2\text{O}_5$ reactivity on steady state

197 In order to further explore the impacting factors on steady state fit method, $\gamma_{ss}(\text{N}_2\text{O}_5)$ results
198 are derived for each 2-hour time period of PKU2017 and TZ2018 dataset based on output from
199 steady state model. Since the pre-set $\gamma(\text{N}_2\text{O}_5)$ in this model is 0.02, the degree of deviation
200 from this value is supposed to reflect the accuracy of the fitted result.

201 It can be noticed from Eq. (2) that the variability of $k\text{NO}_3$ during the same time period
202 leads data points to scatter on lines with different slopes, which could bias the resulted $\gamma_{ss}(\text{N}_2\text{O}_5)$
203 from model pre-set value. As is shown in Figure 3, the absolute percentages of $\gamma_{ss}(\text{N}_2\text{O}_5)$
204 deviation grow dramatically with the increase of relative standard deviation of $k\text{NO}_3$ ($k\text{NO}_3$
205 RSD) in both of winter and summer data sets. The positive correlation even gives rise to
206 extreme deviation in summer data set with up to almost 10 times of model setting $\gamma(\text{N}_2\text{O}_5)$. In
207 fact, there remains accurate $\gamma_{ss}(\text{N}_2\text{O}_5)$ values derived in each range of $k\text{NO}_3$ RSD, indicating a
208 not strictly positive correlation between $\gamma_{ss}(\text{N}_2\text{O}_5)$ deviation and $k\text{NO}_3$ RSD. It implies that
209 large variation of $k\text{NO}_3$ only enhance the possibilities of inaccurate results from steady state
210 fit rather than hinder the $\gamma_{ss}(\text{N}_2\text{O}_5)$ quantification all the time. This phenomenon can only be
211 accounted by the distribution of $k\text{NO}_3$ values point by point.



212



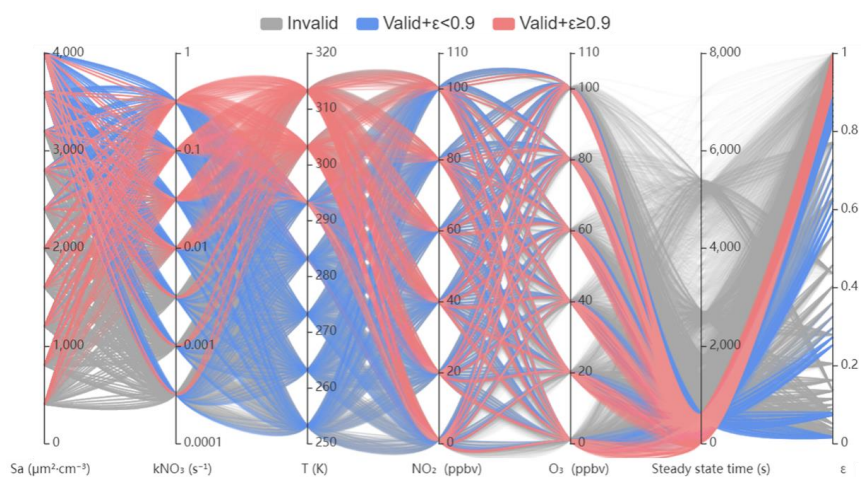
213 **Figure 3.** Relationship between $\gamma(\text{N}_2\text{O}_5)$ derivation through steady state approximation and $k\text{NO}_3$ relative
214 standard deviation (RSD) in box whisker plot. The blue and green color represent dataset from PKU2017
215 and TZ2018 respectively, binned according to $k\text{NO}_3$ RSD. The dots are the mean deviation of $\gamma_{\text{ss}}(\text{N}_2\text{O}_5)$.
216 The number above the box whisker represents the valid data points in each bin.

217 Besides the large variation of $k\text{NO}_3$ in short time period, the absolute level of $k\text{NO}_3$ and
218 $k\text{N}_2\text{O}_5$ could influence the possibilities of inaccurate $\gamma_{\text{ss}}(\text{N}_2\text{O}_5)$ from different aspects.
219 Although the enhancement of $k\text{NO}_3$ and $k\text{N}_2\text{O}_5$ boost the approach to steady state (Text. S5
220 and Figure S7), higher levels of $k\text{NO}_3$ amplify the bias of $\gamma_{\text{ss}}(\text{N}_2\text{O}_5)$, contrary to $k\text{N}_2\text{O}_5$, with
221 the same relative variation of $k\text{NO}_3$ (Text. S6 and Figure S9). It indicates that the region with
222 plural emissions might not be suited for steady state fit due to the high $k\text{NO}_3$. Therefore, a
223 trade-off between the variation of $k\text{NO}_3$ and the high level of $k\text{NO}_3$ (fast approach to steady
224 state) should be made when derive $\gamma_{\text{ss}}(\text{N}_2\text{O}_5)$.

225 3.3 Implication for accurate steady state analysis of $\text{NO}_3\text{-N}_2\text{O}_5$

226 While a few previous researches have examined the validity of steady state under certain
227 conditions via numerical modeling when interpreted the ambient data (Brown et al., 2009;
228 Brown et al., 2003), a clear range well suited to steady state analysis of $\text{NO}_3\text{-N}_2\text{O}_5$, taking both
229 K_{eq} and validity of steady state into consideration, has not been determined to date.

230 Almost 20000 simulations are displayed in the parallel plot of Figure 4, where each line
231 connects 5 constraint parameters to the calculated steady state time and ϵ . The steady state is
232 validated by the approach to steady state within 600 s and the accurate K_{eq} coefficient is
233 defined as ϵ larger than 0.9. The pink and blue lines together represent the conditions valid
234 for steady state without consideration of accurate K_{eq} . While the level of T, NO_2 and O_3 have
235 minor effect on the approach to steady state, simultaneous low $k\text{N}_2\text{O}_5$ (indicated as low Sa in
236 the plot) and $k\text{NO}_3$ prevent the $\text{NO}_3\text{-N}_2\text{O}_5$ system from developing steady state. For example,
237 when $k\text{NO}_3$ is lower than 0.01 s^{-1} , the air mass will be valid only if Sa increases to at least
238 $3000 \mu\text{m}^2 \text{ cm}^{-3}$ with $\gamma(\text{N}_2\text{O}_5)$ of 0.02. It implies that clean air mass is not suited for steady state
239 in any cases, whereas high aerosol condition provides more possibilities to approach steady
240 state even with low $k\text{NO}_3$. However, in order to interpreting $\text{NO}_3\text{-N}_2\text{O}_5$ chemistry with accurate
241 K_{eq} coefficient, the ϵ larger than 0.9 is additionally taken into consideration, which excludes
242 50% of valid steady state cases mainly with high aerosol and lower than 10°C . These cases
243 could bias $[\text{N}_2\text{O}_5]/([\text{NO}_2] \times [\text{NO}_3])$ from original K_{eq} (also indicated in Figure 2), leading to
244 inaccurate results of calculation based on K_{eq} .



245

246 **Figure 4.** Numerical simulations for determining conditions available for steady state approximation
247 method in a parallel axis plot. The first five axes from the left represent initial variables used for constraining
248 the simulations respectively. The last two axes represent the time required for achieving steady state and the
249 ϵ value calculated from the simulated results. The gray lines show cases unable approach steady state within
250 600 s. The blue lines show valid steady state cases with ϵ less than 0.9, which is also inappropriate for
251 steady state analysis. The pink lines show valid steady state cases with ϵ higher than 0.9, which is suited
252 for steady state analysis.

253

In summary, we found that the parameterized K_{eq} coefficient deviates much from the ratio
254 of $[N_2O_5]/([NO_2] \times [NO_3])$ in some cases where steady state is valid. The indicator of the
255 deviation, ϵ , is relatively sensitive to N_2O_5 reactivity and ambient temperature. It implies that
256 conditions suited for steady state analysis should be determined according to not only the
257 validity of steady state but also K_{eq} especially under high aerosol conditions, like some regions
258 in India, China, Europe and the US (Baasandorj et al., 2017; Cesari et al., 2018; Huang et al.,
259 2014; Mogno et al., 2021; Petit et al., 2017; Wang et al., 2017b). Considering that high level of
260 kNO_3 might amplify the bias of $\gamma_{ss}(N_2O_5)$ yield from steady state fit and appears to be
261 accompanied with fast variations, air mass of kNO_3 less than 0.01 s^{-1} with high aerosol and T
262 higher than 10°C is therefore the best suited for steady state analysis of NO_3 - N_2O_5 chemistry,
263 which indicates that this method would be more applicable in polluted regions with high
264 aerosol loading during summertime. If the restriction of ϵ is relaxed to 30%, some of winter
265 conditions will also be applicable. Our results provide an insight to improve the accuracy of
266 steady state approximation method and find suited areas to interpret nighttime chemistry.
267 Further improvement of in-situ NO_3 - N_2O_5 budgets quantification relies on the direct
268 measurements via flow tube system or machine learning prediction based on ancillary
269 parameters.



270

271 **Supporting Information:** The Supporting Information is available on line.

272 Description of the invalid ambient case for NO₃-N₂O₅ steady state analysis (Text S1),
273 description of observation datasets from field campaigns 2017PKU and 2018TZ (Text S2),
274 description of nighttime NO₃-N₂O₅ loss pathway two half-artificial dataset (Text S3),
275 parameterization of Keq coefficient in different databases (Text S4), sensitivity tests of time
276 to approach steady state (Text S5), description of the impacts of *k*NO₃ and *k*N₂O₅ levels on
277 $\gamma_{ss}(N_2O_5)$ (Text S6), related Figures and Tables support the analysis in the text.

278

279 **Code/Data availability.** The datasets used in this study are available from the corresponding
280 author upon request (wanghch27@mail.sysu.edu.cn; k.lu@pku.edu.cn).

281

282 **Author contributions.** K.D.L. and H.C.W. designed the study. X.R.C and H.C.W. analyzed
283 the data and wrote the paper with input from K.D.L.

284

285 **Competing interests.** The authors declare that they have no conflicts of interest.

286

287 **Acknowledgments.** This project is supported by the National Natural Science Foundation of
288 China (21976006, 41907185); the Beijing Municipal Natural Science Foundation for
289 Distinguished Young Scholars (JQ19031); the special fund of the State Key Joint Laboratory
290 of Environment Simulation and Pollution Control (21K02ESPCP); the National Research
291 Program for Key Issue in Air Pollution Control (DQGG0103-01, 2019YFC0214800). Thanks
292 for the data contributed by field campaign team.

293

294 **References**

- 295 Allan, B. J., Carslaw, N., Coe, H., Burgess, R. A., and Plane, J. M. C.: Observations of the Nitrate Radical in the
296 Marine Boundary Layer, *J. Atmos. Chem.*, 33, 129-154, 1999.
- 297 Allan, B. J., McFiggans, G., Plane, J. M. C., Coe, H., and McFadyen, G. G.: The nitrate radical in the remote
298 marine boundary layer, *J. Geophys. Res.: Atmos.*, 105, 24191-24204, 10.1029/2000JD900314, 2000.
- 299 Baasandorj, M., Hoch, S. W., Bares, R., Lin, J. C., Brown, S. S., Millet, D. B., Martin, R., Kelly, K., Zarzana, K.
300 J., Whiteman, C. D., Dube, W. P., Tonnesen, G., Jaramillo, I. C., and Sohl, J.: Coupling between Chemical and
301 Meteorological Processes under Persistent Cold-Air Pool Conditions: Evolution of Wintertime PM_{2.5} Pollution
302 Events and N₂O₅ Observations in Utah's Salt Lake Valley, *Environmental Science & Technology*, 51, 5941-5950,
303 10.1021/acs.est.6b06603, 2017.
- 304 Brown, S. S., Stark, H., and Ravishankara, A. R.: Applicability of the steady state approximation to the
305 interpretation of atmospheric observations of NO₃ and N₂O₅, *J. Geophys. Res.- Atmos.*, 108,



- 306 10.1029/2003jd003407, 2003.
- 307 Brown, S. S., Ryerson, T. B., Wollny, A. G., Brock, C. A., Peltier, R., Sullivan, A. P., Weber, R. J., Dube, W. P.,
308 Trainer, M., Meagher, J. F., Fehsenfeld, F. C., and Ravishankara, A. R.: Variability in nocturnal nitrogen oxide
309 processing and its role in regional air quality, *Science*, 311, 67-70, 10.1126/science.1120120, 2006.
- 310 Brown, S. S., Dube, W. P., Fuchs, H., Ryerson, T. B., Wollny, A. G., Brock, C. A., Bahreini, R., Middlebrook, A.
311 M., Neuman, J. A., Atlas, E., Roberts, J. M., Osthoff, H. D., Trainer, M., Fehsenfeld, F. C., and Ravishankara, A.
312 R.: Reactive uptake coefficients for N₂O₅ determined from aircraft measurements during the Second Texas Air
313 Quality Study: Comparison to current model parameterizations, *J. Geophys. Res. - Atmos.*, 114, D00F10(01-16),
314 Artn D00f10
315 10.1029/2008jd011679, 2009.
- 316 Brown, S. S., Dubé, W. P., Peischl, J., Ryerson, T. B., Atlas, E., Warneke, C., de Gouw, J. A., te Lintel Hekkert,
317 S., Brock, C. A., Flocke, F., Trainer, M., Parrish, D. D., Fehsenfeld, F. C., and Ravishankara, A. R.: Budgets for
318 nocturnal VOC oxidation by nitrate radicals aloft during the 2006 Texas Air Quality Study, *J. Geophys. Res.:*
319 *Atmos.*, 116, 10.1029/2011jd016544, 2011.
- 320 Cantrell, C., Davidson, J., McDaniel, A., Shetter, R., and Calvert, J.: The equilibrium constant for N₂O₅ = NO₂
321 + NO₃ - Absolute determination by direct measurement from 243 to 397 K, *The Journal of Chemical Physics*,
322 88, 10.1063/1.454679, 1988.
- 323 Carslaw, N., Plane, J. M. C., Coe, H., and Cuevas, E.: Observations of the nitrate radical in the free troposphere
324 at Izana de Tenerife, *J. Geophys. Res. - Atmos.*, 102, 10613-10622, 10.1029/96jd03512, 1997.
- 325 Cesari, D., De Benedetto, G. E., Bonasoni, P., Busetto, M., Dinoi, A., Merico, E., Chirizzi, D., Cristofanelli, P.,
326 Donato, A., Grasso, F. M., Marinoni, A., Pennetta, A., and Contini, D.: Seasonal variability of PM_{2.5} and PM₁₀
327 composition and sources in an urban background site in Southern Italy, *Sci. Total Environ.*, 612, 202-213,
328 10.1016/j.scitotenv.2017.08.230, 2018.
- 329 Chen, X., Wang, H., Lu, K., Li, C., Zhai, T., Tan, Z., Ma, X., Yang, X., Liu, Y., Chen, S., Dong, H., Li, X., Wu,
330 Z., Hu, M., Zeng, L., and Zhang, Y.: Field Determination of Nitrate Formation Pathway in Winter Beijing,
331 *Environmental Science & Technology*, 54, 9243-9253, 10.1021/acs.est.0c00972, 2020.
- 332 Chen, X. R., Wang, H. C., Liu, Y. H., Su, R., Wang, H. L., Lou, S. R., and Lu, K. D.: Spatial characteristics of
333 the nighttime oxidation capacity in the Yangtze River Delta, China, *Atmos. Environ.*, 208, 150-157,
334 10.1016/j.atmosenv.2019.04.012, 2019.
- 335 Huang, R.-J., Zhang, Y., Bozzetti, C., Ho, K.-F., Cao, J.-J., Han, Y., Daellenbach, K. R., Slowik, J. G., Platt, S.
336 M., Canonaco, F., Zotter, P., Wolf, R., Pieber, S. M., Brun, E. A., Crippa, M., Ciarelli, G., Piazzalunga, A.,
337 Schwikowski, M., Abbazade, G., Schnelle-Kreis, J., Zimmermann, R., An, Z., Szidat, S., Baltensperger, U.,
338 Haddad, I. E., and Prévôt, A. S. H.: High secondary aerosol contribution to particulate pollution during haze
339 events in China, *Nature*, 514, 218-222, 10.1038/nature13774, 2014.
- 340 Li, Z. Y., Xie, P. H., Hu, R. Z., Wang, D., Jin, H. W., Chen, H., Lin, C., and Liu, W. Q.: Observations of N₂O₅
341 and NO₃ at a suburban environment in Yangtze river delta in China: Estimating heterogeneous N₂O₅ uptake
342 coefficients, *J. Environ. Sci.*, 95, 248-255, 10.1016/j.jes.2020.04.041, 2020.
- 343 McDuffie, E. E., Fibiger, D. L., Dubé, W. P., Lopez-Hilfiker, F., Lee, B. H., Thornton, J. A., Shah, V., Jaeglé, L.,
344 Guo, H., Weber, R. J., Michael Reeves, J., Weinheimer, A. J., Schroder, J. C., Campuzano-Jost, P., Jimenez, J. L.,
345 Dibb, J. E., Veres, P., Ebben, C., Sparks, T. L., Wooldridge, P. J., Cohen, R. C., Hornbrook, R. S., Apel, E. C.,
346 Campos, T., Hall, S. R., Ullmann, K., and Brown, S. S.: Heterogeneous N₂O₅ Uptake During Winter: Aircraft
347 Measurements During the 2015 WINTER Campaign and Critical Evaluation of Current Parameterizations, *J.*



- 348 Geophys. Res.: Atmos., 123, 4345-4372, 10.1002/2018jd028336, 2018.
- 349 McDuffie, E. E., Womack, C. C., Fibiger, D. L., Dube, W. P., Franchin, A., Middlebrook, A. M., Goldberger, L.,
350 Lee, B. H., Thornton, J. A., Moravek, A., Murphy, J. G., Baasandorj, M., and Brown, S. S.: On the contribution
351 of nocturnal heterogeneous reactive nitrogen chemistry to particulate matter formation during wintertime
352 pollution events in Northern Utah, Atmos. Chem. Phys., 19, 9287-9308, 10.5194/acp-19-9287-2019, 2019.
- 353 Mogno, C., Palmer, P. I., Knote, C., Yao, F., and Wallington, T. J.: Seasonal distribution and drivers of surface
354 fine particulate matter and organic aerosol over the Indo-Gangetic Plain, Atmos. Chem. Phys., 21, 10881-10909,
355 10.5194/acp-21-10881-2021, 2021.
- 356 Morgan, W. T., Ouyang, B., Allan, J. D., Aruffo, E., Di Carlo, P., Kennedy, O. J., Lowe, D., Flynn, M. J.,
357 Rosenberg, P. D., Williams, P. I., Jones, R., McFiggans, G. B., and Coe, H.: Influence of aerosol chemical
358 composition on N₂O₅ uptake: airborne regional measurements in northwestern Europe, Atmos. Chem. Phys., 15,
359 973-990, 10.5194/acp-15-973-2015, 2015.
- 360 Osthoff, H. D., Sommariva, R., Baynard, T., Pettersson, A., Williams, E. J., Lerner, B. M., Roberts, J. M., Stark,
361 H., Goldan, P. D., Kuster, W. C., Bates, T. S., Coffman, D., Ravishankara, A. R., and Brown, S. S.: Observation
362 of daytime N₂O₅ in the marine boundary layer during New England Air Quality Study - Intercontinental
363 Transport and Chemical Transformation 2004, J. Geophys. Res.- Atmos., 111, 10.1029/2006jd007593, 2006.
- 364 Petit, J. E., Amodeo, T., Meleux, F., Bessagnet, B., Menut, L., Grenier, D., Pellan, Y., Ockler, A., Rocq, B., Gros,
365 V., Sciare, J., and Favez, O.: Characterising an intense PM pollution episode in March 2015 in France from multi-
366 site approach and near real time data: Climatology, variabilities, geographical origins and model evaluation,
367 Atmos. Environ., 155, 68-84, 10.1016/j.atmosenv.2017.02.012, 2017.
- 368 Phillips, G. J., Thieser, J., Tang, M., Sobanski, N., Schuster, G., Fachinger, J., Drewnick, F., Borrmann, S.,
369 Bingemer, H., Lelieveld, J., and Crowley, J. N.: Estimating N₂O₅ uptake coefficients using ambient measurements
370 of NO₃, N₂O₅, ClNO₂ and particle-phase nitrate, Atmos. Chem. Phys., 16, 13231-13249, 10.5194/acp-16-13231-
371 2016, 2016.
- 372 Platt, U. F., Winer, A. M., Biermann, H. W., Atkinson, R., and Pitts, J. N.: Measurement of nitrate radical
373 concentrations in continental air, Environmental Science & Technology, 18, 365-369, 10.1021/es00123a015,
374 1984.
- 375 Pritchard, H.: The nitrogen pentoxide dissociation equilibrium, Int. J. Chem. Kinet., 26, 61-71,
376 10.1002/kin.550260108, 1994.
- 377 Stutz, J., Alicke, B., Ackermann, R., Geyer, A., White, A., and Williams, E.: Vertical profiles of NO₃, N₂O₅, O-
378 3, and NO_x in the nocturnal boundary layer: 1. Observations during the Texas Air Quality Study 2000, J. Geophys.
379 Res.- Atmos., 109, 10.1029/2003jd004209, 2004.
- 380 Vrekoussis, M., Mihalopoulos, N., Gerasopoulos, E., Kanakidou, M., Crutzen, P. J., and Lelieveld, J.: Two-years
381 of NO₃ radical observations in the boundary layer over the Eastern Mediterranean, Atmos. Chem. Phys., 7, 315-
382 327, 10.5194/acp-7-315-2007, 2007.
- 383 Wagner, N. L., Riedel, T. P., Young, C. J., Bahreini, R., Brock, C. A., Dubé, W. P., Kim, S., Middlebrook, A. M.,
384 Öztürk, F., Roberts, J. M., Russo, R., Sive, B., Swarthout, R., Thornton, J. A., VandenBoer, T. C., Zhou, Y., and
385 Brown, S. S.: N₂O₅ uptake coefficients and nocturnal NO₂ removal rates determined from ambient wintertime
386 measurements, J. Geophys. Res.: Atmos., 118, 9331-9350, 10.1002/jgrd.50653, 2013.
- 387 Wang, H., Lu, K., Chen, X., Zhu, Q., Chen, Q., Guo, S., Jiang, M., Li, X., Shang, D., Tan, Z., Wu, Y., Wu, Z.,
388 Zou, Q., Zheng, Y., Zeng, L., Zhu, T., Hu, M., and Zhang, Y.: High N₂O₅ Concentrations Observed in Urban
389 Beijing: Implications of a Large Nitrate Formation Pathway, Environ Sci Tech Let, 4, 416-420,



390 10.1021/acs.estlett.7b00341, 2017a.
391 Wang, H. C., Lu, K. D., Chen, X. R., Zhu, Q. D., Wu, Z. J., Wu, Y. S., and Sun, K.: Fast particulate nitrate
392 formation via N₂O₅ uptake aloft in winter in Beijing, *Atmos. Chem. Phys.*, 18, 10483-10495, 10.5194/acp-18-
393 10483-2018, 2018a.
394 Wang, H. C., Lu, K. D., Guo, S., Wu, Z. J., Shang, D. J., Tan, Z. F., Wang, Y. J., Le Breton, M., Lou, S. R., Tang,
395 M. J., Wu, Y. S., Zhu, W. F., Zheng, J., Zeng, L. M., Hallquist, M., Hu, M., and Zhang, Y. H.: Efficient N₂O₅
396 uptake and NO₃ oxidation in the outflow of urban Beijing, *Atmos. Chem. Phys.*, 18, 9705-9721, 10.5194/acp-
397 18-9705-2018, 2018b.
398 Wang, J., Zhao, B., Wang, S., Yang, F., Xing, J., Morawska, L., Ding, A., Kulmala, M., Kerminen, V.-M.,
399 Kujansuu, J., Wang, Z., Ding, D., Zhang, X., Wang, H., Tian, M., Petäjä, T., Jiang, J., and Hao, J.: Particulate
400 matter pollution over China and the effects of control policies, *Sci. Total Environ.*, 584-585, 426-447,
401 <https://doi.org/10.1016/j.scitotenv.2017.01.027>, 2017b.
402 Wang, S., Shi, C., Zhou, B., Zhao, H., Wang, Z., Yang, S., and Chen, L.: Observation of NO₃ radicals over
403 Shanghai, China, *Atmos. Environ.*, 70, 401-409, 10.1016/j.atmosenv.2013.01.022, 2013.
404 Wang, X., Wang, H., Xue, L., Wang, T., Wang, L., Gu, R., Wang, W., Tham, Y. J., Wang, Z., Yang, L., Chen, J.,
405 and Wang, W.: Observations of N₂O₅ and ClNO₂ at a polluted urban surface site in North China: High N₂O₅
406 uptake coefficients and low ClNO₂ product yields, *Atmos. Environ.*, 156, 125-134,
407 10.1016/j.atmosenv.2017.02.035, 2017c.
408 Wang, Y., Yao, L., Wang, L., Liu, Z., Ji, D., Tang, G., Zhang, J., Sun, Y., Hu, B., and Xin, J.: Mechanism for the
409 formation of the January 2013 heavy haze pollution episode over central and eastern China, *Science China Earth*
410 *Sciences*, 57, 14-25, 10.1007/s11430-013-4773-4, 2014.
411 Wang, Z., Wang, W., Tham, Y. J., Li, Q., Wang, H., Wen, L., Wang, X., and Wang, T.: Fast heterogeneous N₂O₅
412 uptake and ClNO₂ production in power plant and industrial plumes observed in the nocturnal residual layer over
413 the North China Plain, *Atmos. Chem. Phys.*, 17, 12361-12378, 10.5194/acp-17-12361-2017, 2017d.
414 Yu, C., Wang, Z., Xia, M., Fu, X., Wang, W., Yee Jun, T., Chen, T., Zheng, P., Li, H., Shan, Y., Wang, X., Xue,
415 L., Zhou, Y., Yue, D., Ou, Y., Gao, J., Lu, K., Brown, S., Zhang, Y., and Tao, W.: Heterogeneous N₂O₅ reactions
416 on atmospheric aerosols at four Chinese sites: improving model representation of uptake parameters, *Atmos.*
417 *Chem. Phys.*, 20, 4367-4378, 10.5194/acp-20-4367-2020, 2020.
418